Journal of Radiation Research, Vol. 58, No. 5, 2017, pp. 755–760
doi: 10.1093/jrr/rrx036
Advance Access Publication: 28 July 2017

Development of a minipig physical phantom from CT data

Sooyeun Park[1,2], Pilsoo Lee[1], Wi-Ho Ha[1,*], Han Sung Kim[1], Byeong Ryong Park[1], Jae Seok Kim[1], Sehwan Shim[3], Sunhoo Park[3], Young-su Kim[2], Chan Hyeong Kim[2] and Young-Woo Jin[4]

[1]Laboratory of Health Physics, National Radiation Emergency Medical Center, Korea Institute of Radiological and Medical Sciences, 75 Nowon-gil, Nowon-gu 01812, Seoul, Republic of Korea
[2]Department of Nuclear Engineering, Hanyang University, 04763, 222 Wangsimni-ro, Seongdong-gu, Seoul, Republic of Korea
[3]Laboratory of Radiation Exposure & Therapeutics, National Radiation Emergency Medical Center, Korea Institute of Radiological and Medical Sciences, 75 Nowon-gil, Nowon-gu 01812, Seoul, Republic of Korea
[4]National Radiation Emergency Medical Center, Korea Institute of Radiological and Medical Sciences, 75 Nowon-gil, Nowon-gu 01812, Seoul, Republic of Korea
*Corresponding author. Department of Health Physics, National Radiation Emergency Medical Center, Korea Institute of Radiological and Medical Sciences, 75 Nowon-gil, Nowon-gu 01812, Seoul, Republic of Korea. Tel: +82-2-3399-5961; Fax: +82-2-3399-5960; Email: lovin@kirams.re.kr
Received January 18, 2017; Revised April 27, 2017; Editorial Decision June 15, 2017

ABSTRACT

Quantification of pathological progression of radiation-induced injury is essential in development of treatment methods, and a proper animal model is necessary for relevant radiological and medical studies. A minipig is a current animal model selected because of its similarities to humans in anatomy and pathology. In the present study, a minipig physical phantom was developed using computed tomography (CT) data. For dosimetry purposes, the minipig physical phantom was constructed on a slice-by-slice basis, with an array of holes to accommodate dosimeters. The phantom is constituted of three major organs, i.e. bone, lung, and remaining soft tissue, and the organs are clearly distinguishable on each 20-mm-thick axial slice. The quality of the tissue-equivalent (TE) substitutes was analyzed in terms of the atomic compositions and Hounsfield units (HUs). The density (in g/cm^3) and effective atomic number of TE substitutes for the bone, lung, and soft tissue are 1.4 and 7.9, 0.5 and 10.0, and 1.0 and 5.9, respectively. Although the TE substitutes have slightly different physical properties, we think the phantom is acceptable because the HU values of the TE substitutes lie in the HU range of real tissues.

KEYWORDS: minipig, physical phantom, tissue-equivalent material, radiation dosimetry, minipig physical phantom

INTRODUCTION

Even though quantification of the pathological progression of radiation-induced injury is essential in the development of new drugs and treatment methods [1], it is difficult to achieve due to the lack of clinical cases. As a result, rodent models have been widely used in preclinical studies, and rodent physical phantoms have been developed and used to measure dose distribution in the body [2].

Due to the much smaller anatomic dimensions of a rodent, however, the extrapolation of the dose–response relationship obtained with rodent models to humans is often accompanied by large uncertainties [3, 4]. In addition, most commercially available mouse physical phantoms are developed in a simplified stylized geometry, causing additional uncertainties in dose calculation [5–7]. Therefore, we believe it is beneficial to develop a realistic phantom of an appropriate medium-sized animal model for more accurate translational research on radiation injury. Köhn *et al.* suggested that a minipig is an appropriate animal model for conducting medical experiments [8], and some researchers are now using a minipig model for radiological and medical studies, e.g. a study on radiation-induced lung injury [1].

In the present study, therefore, we have developed a minipig physical phantom for radiation dosimetry purposes, using the computed tomography (CT) data of a real minipig. The physical phantom replicates both the internal and external features of a real minipig, reflecting the intricate anatomy and density inhomogeneity. Here, we present the detailed procedure for constructing the physical phantom, together with its characteristics. Also, the quality of the tissue-equivalent (TE) materials was analyzed in terms of the atomic compositions and Hounsfield units.

MATERIALS AND METHODS

Model preparation

A Göttingen minipig, which was demonstrated to be pathogen-free in molecular biology and clinical pathology tests, was recruited as a model for the construction of a physical phantom. The weight and age of the minipig were 20 kg and 7 months, respectively (considered to be appropriate for the relevant clinical research involving radiation exposure) [9–14]. The present study was reviewed and approved by the Institutional Animal Care and Use Committee (IACUC) of Korea Institute of Radiological and Medical Sciences (KIRAMS #2016-0011). In order to reproduce the bodily structures of the minipig, computed tomography (CT) images were taken using a helical CT scanner, Asteion 4 (TOSHIBA, Japan). An X-ray tube was set at 150 kVp and 12 mAs, and CT images with a resolution of 512 × 512 pixels were generated with a 2.5 mm slice thickness. On the basis of the accumulated CT images, a reconstruction of a 3D minipig model was carried out.

As the first step toward creating a 3D minipig model, lung, bone, and soft-tissue regions were distinguished in terms of the Hounsfield units (HUs) recorded in the digital imaging and communications in medicine (DICOM) data, and were subsequently used to generate 3D mesh models. The organs were automatically segmented by using the OnDemand (CyberMed, Korea) software, and the resulting 3D meshes were exported into the stereolithography (STL) format. The process of 3D modeling is shown in Fig. 1.

Because the initially generated 3D organ models were found to have geometrical defects (such as irregular indention, false looping, self-overlapping and local discontinuities), the defects were manually fixed by using the general-purpose computer-aided design (CAD) software Rhinoceros (Robert McNeel & Associates, Seattle). After the 3D organ models were properly constructed, the entire body was sliced into 27 pieces, except for the head and tail; then, each slice was designed to have dosimeter holes in a grid pattern. Finally, the constructed 3D organ models were translated into the standard format for the exchange of product model data (STEP) to create gcode, which contains all the types of information required for precision milling machines. In addition, a minipig computational phantom was developed based on the minipig 3D model having segmented organs for being used in computational dosimetry.

Tissue-equivalent substitute selection

In the present minipig model, two organs (i.e., the lung and bone) were distinguished, and the other organ were simply represented by soft tissue. Because the organs incorporated in a physical phantom are made of TE substitutes (representing real tissues in the minipig), the selection of appropriate TE materials pertinent to radiological study is critical in the development of a physical phantom.

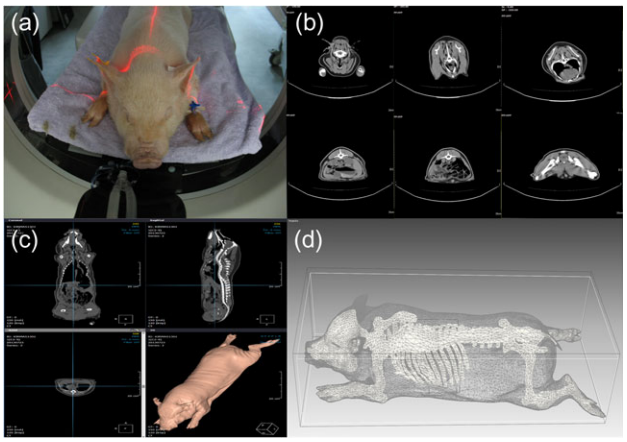

Fig. 1. Steps for converting the 3D stereolithography (STL) polygonal image data based on minipig CT images using the OnDemand software: (a) anatomical data acquisition via CT examination, (b) the resulting CT images, (c) 3D rendering in the OnDemand software, and (d) a reconstructed 3D minipig polygonal model.

In the case of human tissues, the physical properties related to radiation are thoroughly tabulated [15, 16], and the corresponding TE materials that can be used for building a physical phantom have been studied as well [15–17]. On the contrary, information on animal tissues is scarce, and it is rather common to use data on human tissues for animal computational phantoms [4, 18]. For this reason, the TE materials used for the present physical phantom were selected on the basis of the well-established data for human tissues.

A number of commercially available materials were examined for the TE materials; consequently, several candidates were initially chosen on the basis of their mass density, rigidity, and colors. In order to use the TE materials in the manufacturing processes of a medium-sized minipig phantom, they had to be cost effective and convenient to handle. Among the TE candidates, the most appropriate materials satisfying our requirements were selected.

Prior to fabrication, the atomic constituents of the selected TE materials were investigated by means of inductively coupled plasma-mass spectroscopy (ICP-MS), ion chromatography, and elemental analysis at the Korea Polymer Testing and Research Institute (KOPTRI) [19]. The elemental compositions and mass densities of the TE substitutes are tabulated in Table 1 in comparison with the International Commission on Radiation Units and Measurements (ICRU) human-tissue counterparts [15]. The effective atomic number Z_{eff} of the TE substitutes were calculated using the formula of Mayneord [20],

$$Z_{\text{eff}} = \sqrt[2.94]{\sum f_i Z_i^{2.94}},$$

Table 1. Mass fraction (in percentages) for major atomic elements and mass density of current tissue-equivalent materials in comparison with the ICRU human-tissue counterparts [15]

Material	soft tissue		bone		lung	
Element	This	ICRU	This	ICRU	This	ICRU
H	8.1	10.5	4.5	3.5	4.8	10.3
C	85.4	25.6	56.7	16.0	36.9	10.5
N	5.9	2.7	0.1	4.2	3.6	3.1
O	0.5	60.2	22.4	44.5	9.3	74.9
B	0.0	0.0	0.0	0.0	5.5	0.0
Mg	0.1	0.0	2.1	0.2	0.8	0.0
Si	0.0	0.0	0.1	0.0	16.4	0.0
Ca	0.1	0.0	1.8	21.5	0.3	0.0
Density (g/cm^3)	**1.0**	**1.0**	**1.4**	**1.3**	**0.5**	**0.3**
Z_{eff}	**5.9**	**7.2**	**7.9**	**13.0**	**10.0**	**7.5**

where f_i and Z_i are the weight fraction of the total number of electrons and the atomic number of element i, respectively.

Soft-tissue-equivalent substitute

Acrylonitrile butadiene styrene (ABS) has a mass density that is similar to that of human soft tissue (1.04 g/cm^3). It was demonstrated that ABS also has dosimetry-related physical properties—in addition to the mass density—that are comparable with commonly used TE materials such as polymethyl methacrylate (PMMA), polystyrene, and solid water (WT1) [21]. Thus, soft tissue, which accounts for the largest fraction of the minipig phantom, was substituted with ABS, considering the radiological properties and fabrication processes.

Bone-tissue–equivalent substitute

The bone region in the real minipig was simplified with homogeneous bone that has a mass density comparable with the average mass density of human tissues [15]. Regarding the bone TE material, a fiber-reinforced plastic (FRP), Polycoat CH-304 (Aekyung, Korea), was selected as a base material; then, it was admixed with talcum powder at a 7:3 weight ratio to adjust the mass density of the resulting material.

Lung-tissue–equivalent substitute

Non-foaming urethane, which has a low mass density and sufficient hardness to maintain the shape of a lung, was chosen to be a lung TE substitute. In the fabrication processes, clay-type non-foaming urethane, X1617 (Nissin Resin, Japan), was blended with a hardening agent at a 5:5 weight ratio.

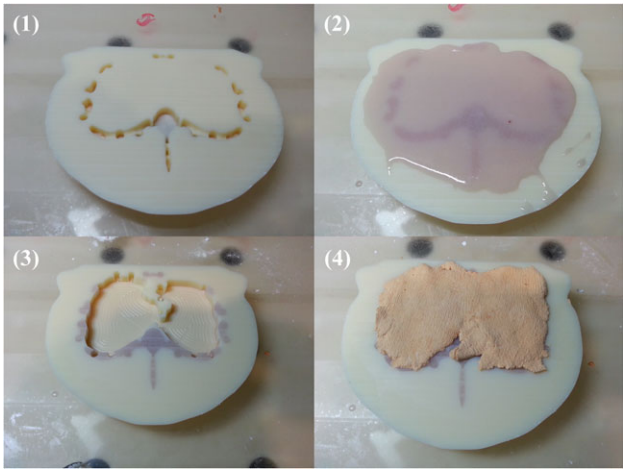

Fig. 2. Progression of phantom construction. (1) Soft-tissue frames were first manufactured; then, the bone regions were chiseled away using a five-axis computer numerical controlled machine in preparation for pouring a bone TE substitute. (2) A bone TE substitute was poured into the mold and cured for a day. (3) After curing, the lung molds were created, and (4) the lung TE substitute was filled in the lung region.

Fabrication processes

At the beginning of the fabrication processes, all soft-tissue frames were created by employing a five-axis computerized-numerical-controlled (CNC) machine, HWG-60M (Hans Machine, Korea), in conjunction with PowerMill (Autodesk, California) computer-aided-manufacturing (CAM) software. The five-axis CNC machine moves the machining centers along five axes (three ordinary Cartesian axes and two additional rotation axes), allowing complicated geometries to be carved as end mills approach an object from all directions. The end mill was operated at 24 000 rpm, with a feed rate of 12 m/min on a 20-mm-thick ABS board. The soft-tissue frames were created slice by slice to ensure clean surfaces.

Shortly afterward, the created soft-tissue frames were tightly anchored to an ABS board using jig pins, and the bone-tissue regions were chiseled away to create molds for bone tissue. Then, the bone TE substitute was overfilled into the molds and cured for a day. The procedure for creating the bone region was repeated to create the lung region in the same manner. After creating the lung molds, a clay-type lung TE substitute was manually kneaded and slightly overfilled into the lung region. After 24 h of curing, the overfilled bone and lung TE substitutes were sanded to be flush with the surface. The entire procedure for fabricating the axial slices is shown in Fig. 2. After removing the jig pins, the fabricated axial slices were detached from the ABS board; subsequently, dosimeter holes were drilled.

RESULTS AND DISCUSSION

By taking advantage of commercial CAD tools and advanced milling techniques, we were able to construct a minipig physical phantom

including specific anatomical details (Fig. 3b). The weight of the whole phantom was 20.0 kg, and the size from head to toe corresponded to 922.0 mm, while each volume (weight) of the TE materials was 949.1 (0.493), 1554.0 (2.160) and 17 047.4 cm^3 (17.388 kg) for lung, bone, and soft tissue, respectively. The constructed physical phantom then underwent CT examination for verification. In the CT topogram, the lung, bone, and soft-tissue regions were clearly separated. However, because the physical phantom was sliced into 27 pieces from head to tail, dark lines arising from the air gaps between slices appeared in the topogram (Fig. 3c).

Mortise and tenon structures were introduced in the present physical phantom. Figure 4 shows the tenon inserted into the mortise from the ventral side. Compared with previous physical phantoms, which used a reinforced top or thread assembly for supporting structures [22–24], the mortise and tenon allowed the physical phantom to be securely anchored and readily disassembled. The mortise and tenon structures were not expected to significantly perturb the dose distribution inside the phantom because, for a fixed position of this phantom, it was intended to irradiate the phantom vertically or laterally from the top. Moreover, any additional dose that might be induced by the secondary radiations scattered from the mortise and tenon structures could be deduced by using the simultaneously developed computational phantom excluding the structures.

For dosimetric purposes, 7-mm-diameter holes, into which radiation dosimeters and their corresponding holders can be inserted, were drilled in a grid pattern in each slice (Fig. 5a). Holders were prepared for rod-type glass or chip-type alanine dosimeters in order to accommodate dosimeters of different shapes and sizes. The dosimeter holes are to be filled with solid plugs made of TE substitutes when no dosimeters are present (Fig. 5b). The total number of dosimeter holes is 2628, although the number in each axial slice differs slightly from slice to slice.

The mass density generally agrees well with the reference values, whereas the mass fractions for the major atomic constituents differ from the ICRU values. Aside from the elements listed in Table 1, the TE materials are found to have small amounts of heavier atomic elements, which were not intended to be included in the fabrication processes. The sources of such elements are unclear for now; however, it is suspected that some of them could be derived from the adhesive and hardening agents. As a result, the effective atomic number of lung became greater than that of bone, which might affect dosimetry results, especially with radiations in a low-energy domain.

For evaluating the response to diagnostic radiation fields (e.g. low-energy photons) of the TE substitutes quantitatively with respect to those of the real tissues in a minipig, the HU values were investigated by analyzing the CT data of the constructed physical phantom and a real minipi, using Amide's a Medical Imaging Data Examiner (AMIDE) software. In the case of the real minipig, the HU values for the lung, spine and thigh are determined to be within the widely accepted HU ranges [25] and are calculated to be −807.17, 19.67 and 448.71 (black lines in Fig. 6), respectively. Furthermore, the mean values for the corresponding tissues in the physical phantom, i.e. the lung, bone, and soft tissue, are −556.66, −32.51 and 195.42 (red lines in Fig. 6), respectively. It is worth noting that the HU values of the physical phantom could be obtained after excluding the air gaps between the axial slices from the range of interest (ROI). When the air gaps were included in the ROI for the calculation of the HU values, the deduced values tended to

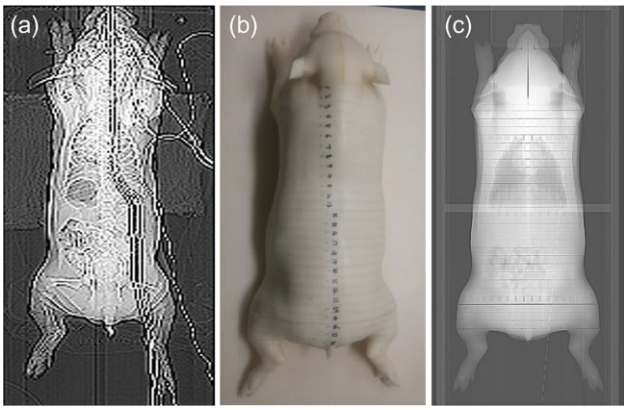

Fig. 3. (a) Topogram of the minipig, (b) a picture taken from above, and (c) a topogram of the constructed physical phantom.

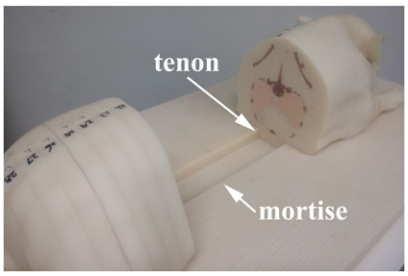

Fig. 4. Axial slices can be securely anchored and readily disassembled without any threaded assembly by introducing a mortise and tenon.

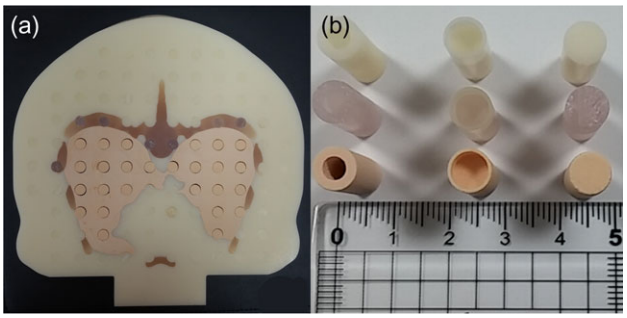

Fig. 5. (a) Every axial slice has dosimeter holes in a grid pattern. As shown in the figure, three different tissues are clearly distinguishable to the naked eye because of the different colors. (b) Two types of dosimeter holders and solid plugs are prepared in the tissue-equivalent materials.

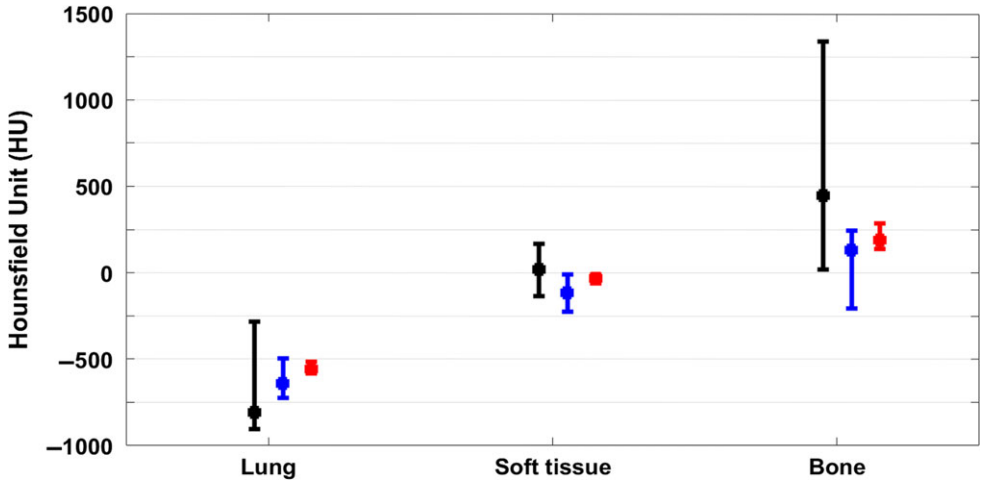

Fig. 6. Comparison of the HU value distributions of the real minipig (black) and the physical phantom, including/excluding (blue/red) the air gaps between axial slices.

decrease slightly compared with the correctly deduced values, owing to the lower attenuation coefficient of air. Given the results of the HU analysis, the present TE materials for the bone and soft tissues reasonably represent the real minipig tissues.

CONCLUSIONS

On the basis of tomographic images of a minipig, we have, for the first time, developed a realistic animal physical phantom for radiation dosimetry. The physical phantom has two major organs, the lung and bone, and the rest of the organ systems were represented by soft tissue. In subsequent CT examination, it was found that the anatomy of the real minipig is replicated well by the physical phantom, where the TE substitutes are made of commercially available high-polymer materials. By analyzing DICOM data, it was shown that the HU values of the TE materials lie in the HU range of real tissues, suggesting that the materials can be substituted for real tissues. Nevertheless, it still remains a challenge to find additional candidate TE materials that can represent real tissues in terms of density and elemental composition. It is expected that the minipig physical phantom will be able to provide experimental values for dose distributions in complicated geometries, and that this will contribute to more accurate dosimetry and preclinical studies.

CONFLICT OF INTEREST

The authors declare that there are no conflicts of interest.

FUNDING

This study was supported by a grant of the Korea Institute of Radiological and Medical Sciences (KIRAMS), funded by Ministry of Science, ICT and Future Planning, Republic of Korea (1711045573; 1711045551/50535-2017).

REFERENCES

1. Lee J-G, Park S, Bae C-H, et al. Development of a minipig model for lung injury induced by a single high-dose radiation exposure and evaluation with thoracic computed tomography. *J Radiat Res* 2016;57:201–09.
2. Welch D, Harken AD, Randers-Pehrson G, et al. Construction of mouse phantoms from segmented CT scan data for radiation dosimetry studies. *Phys Med Biol* 2015;60:3589–98.
3. National Council on Radiation Protection and Measurements. Extrapolation of radiation-induced cancer risks from nonhuman experimental systems to humans. *NCRP Report No. 150*. 2005.
4. Padilla L, Lee C, Milner R, et al. Canine anatomic phantom for preclinical dosimetry in internal emitter therapy. *J Nucl Med* 2008;49:446–52.
5. Anderson-Evans CD. *Estimating Effective Dose from Phantom Dose Measurements in Atrial Fibrillation Ablation Procedures and Comparison of MOSFET and TLD Detectors in a Small Animal Dosimetry Setting*. Durham, North Carolina: Duke University, 2011.
6. Knoess C, Siegel S, Smith A, et al. Performance evaluation of the microPET R4 PET scanner for rodents. *Eur J Nucl Med Mol Imaging* 2003;30:737–47.
7. Stenner P, Berkus T, Kachelriess M. Empirical dual energy calibration (EDEC) for cone-beam computed tomography. *Med Phys* 2007;34:3630–41.
8. Köhn F, Sharifi A, Täubert H, et al. Breeding for low body weight in Goettingen minipigs. *J Anim Breed Genet* 2008;125:20–8.
9. Agay D, Scherthan H, Forcheron F, et al. Multipotent mesenchymal stem cell grafting to treat cutaneous radiation syndrome: development of a new minipig model. *Exp Hematol* 2010;38:945–56.
10. Forcheron F, Agay D, Scherthan H, et al. Autologous adipocyte derived stem cells favour healing in a minipig model of cutaneous radiation syndrome. *PLoS One* 2012;7:e31694.
11. Kim J-W, Lee D-W, Choi W-H, et al. Development of a porcine skin injury model and characterization of the dose-dependent response to high-dose radiation. *J Radiat Res* 2013;54;823–31.
12. Riccobono D, Forcheron F, Agay D, et al. Transient gene therapy to treat cutaneous radiation syndrome: development in a minipig model. *Health Phys* 2014;106:713–9.

13. Shim S, Jang W-S, Lee S-J, et al. Development of a new minipig model to study radiation-induced gastrointestinal syndrome and its application in clinical research. *Radiat Res* 2014;181:387–95.
14. Kim J-S, Rhim K-J, Jang W-S, et al. β-irradiation (^{166}Ho patch)-induced skin injury in mini-pigs: effects on NF-κB and COX-2 expression in the skin. *J Vet Sci* 2015;16:1–9.
15. International Commission on Radiation Units and Measurements. Photon, Electron, Proton and Neutron Interaction Data for Body Tissues. *ICRU Report 46*. Bethesda, 1992.
16. Valentin J. Basic anatomical and physiological data for use in radiological protection: reference values. *Ann ICRP* 2002;32: 3–4.
17. White D, Widdowson E, Woodard H, et al. The composition of body tissues (II). Fetus to young adult. *Br J Radiol* 1991;64: 149–59.
18. Keenan MA, Stabin MG, Segars WP, et al. RADAR realistic animal model series for dose assessment. *J Nucl Med* 2010;51: 471–76.
19. Korea Polymer Testing and Research Institute (KOPTRI). The official homepage Seoul. http://www.polymer.co.kr (18 April 2017, data last accessed).
20. Mayneord W. The significance of the Roentgen. *Acta Int Union Against Cancer* 1937;2:271–82.
21. Kumar R, Sharma S, Deshpande S, et al. Acrylonitrile Butadiene Styrene (ABS) plastic based low cost tissue equivalent phantom for verification dosimetry in IMRT. *J Appl Clin Med Phys* 2009; 11:3030.
22. Nakaguchi Y, Ono T, Maruyama M, et al. Validation of fluence-based 3D IMRT dose reconstruction on a heterogeneous anthropomorphic phantom using Monte Carlo simulation. *J Appl Clin Med Phys* 2015;16:5199.
23. Matsubara K, Koshida H, Sakuta K, et al. Radiation dose and physical image quality in 128-section dual-source computed tomographic coronary angiography: a phantom study. *J Appl Clin Med Phys* 2012;13:3959.
24. Lu H, Zhuo W, Xu B, et al. Organ and effective dose evaluation in coronary angiography by using a 320 MDCT based on in-phantom dose measurements with TLDs. *J Radiol Prot* 2015;35: 597–609.
25. Winslow JF, Hyer DE, Fisher RF, et al. Construction of anthropomorphic phantoms for use in dosimetry studies. *J Appl Clin Med Phys* 2009;10:2986.